Beta-amyloid deposition maps onto hippocampal and subiculum atrophy in dementia with Lewy bodies

Elijah Mak [1], Paul C Donaghy [2], Elizabeth McKiernan [1], Michael J Firbank [2], Jim Lloyd [3], George S Petrides [3], Alan J Thomas [2], John T O'Brien[1]*

AFFILIATIONS

[1] Department of Psychiatry, University of Cambridge, UK

[2] Institute for Ageing and Institute of Neuroscience, Newcastle University, UK

[3] Nuclear Medicine Department, Newcastle upon Tyne Hospitals, NHS Foundation Trust, UK

CORRESPONDING AUTHOR:

John T O'Brien

Foundation Professor of Old Age Psychiatry

Department of Psychiatry

University of Cambridge School of Clinical Medicine

Box 189, Level E4 Cambridge Biomedical Campus

Cambridge

CB2 0SP

UK

ABSTRACT

Although dementia with Lewy bodies (DLB) is a synucleinopathy, it is frequently accompanied by β-amyloid accumulation (Aβ). Elucidating the relationships of Aβ with grey matter atrophy in DLB may yield insights regarding the contributions of comorbid Alzheimer's disease to its disease progression. Twenty healthy controls and twenty-five DLB subjects underwent clinical assessment, [18F]-Florbetapir and 3T MRI. Freesurfer was used to estimate cortical thickness and subcortical volumes and PetSurfer was used to quantify [18F]-Florbetapir standardised uptake value ratio. Principal component analysis was used to identify the dominant Aβ component for correlations with regional cortical thickness, hippocampal subfields and subcortical structures. Relative to healthy controls, the DLB group demonstrated increased Aβ in widespread regions encompassing the frontal and temporo-parietal cortices, whereas cortical thinning was restricted to the temporal lobe. Amongst DLB subjects, the Aβ component was significantly associated with more severe hippocampal and subiculum atrophy. These findings may reflect an early process of superimposed AD-like atrophy in DLB, thereby conferring support for the therapeutic potential of anti-Aβ interventions in people with DLB.

KEYWORDS: Dementia with Lewy bodies, Alzheimer's disease, amyloid, PET, MRI.

1. INTRODUCTION

Dementia with Lewy bodies (DLB) is the second most common degenerative form of dementia in elderly people after Alzheimer's disease (AD) (McKeith et al., 2017). Although alpha-synucleinopathy is recognised as the key neuropathological hallmark of DLB, up to 80% of people with DLB show varying degrees of AD pathologies – beta-amyloid (Aβ) and neurofibrillary tau tangles (NFTs) – at autopsy (Colom-Cadena et al., 2013; McKeith et al., 2017, 2005). The advent of PET amyloid ligands has offered unique opportunities for the ante-mortem quantification of Aβ burden and how it relates to clinical and neuroimaging abnormalities associated with preclinical and established AD (Chetelat *et al.*, 2013; see Habib and Mak *et al.*, 2017 for a systematic review). However, it remains unclear if and to what extent Aβ contributes to the disease progression and neurodegenerative changes in DLB (see Donaghy *et al.*, 2015 for a systematic review). This knowledge gap is unfortunate, since new insights concerning the impact of Aβ in DLB could have long-term ramifications on treatment strategies as well as monitoring outcomes in emerging trials that specifically target the aggregation of Aβ (Sperling et al., 2014).

The 'Aβ cascade hypothesis' in AD posits an initiating event of amyloidosis, with subsequent tau accumulation preceding downstream brain atrophy and cognitive decline (Hardy, 2002). This AD spatio-temporal model of disease progression has been central to the recent shift towards disease-modification strategies (Sperling et al., 2014), although its relevance to DLB is still controversial (Donaghy et al., 2015). For instance, limited evidence suggests a modest association of Aβ with cognitive decline and increased mortality risks (Gomperts, 2014), although others have reported no association with dementia severity in DLB (Shimada et al., 2013). The discordant findings may, in part, stem from the inherent challenges of psychometric assessments such as mood changes, fatigue and attentional impairments, all of which could be exacerbated by cognitive fluctuations in DLB patients. In contrast, particularly in the context of AD, brain atrophy is increasingly proposed as a reliable biomarker of disease progression (Sluimer et al., 2008) and secondary outcome measure in clinical trials (Cash et al., 2015; Schott et al., 2010; Slattery et al., 2015).

Widely understood to be one of endpoints in the neurodegenerative cascade (Jack et al., 2013), brain atrophy has been extensively studied in relation to upstream Aβ across the spectrum of normal ageing, mild cognitive impairment and AD (Chetelat et al., 2010; Josephs et al., 2008). Surprisingly, this question has been scarcely addressed in DLB (Shimada *et al.*, 2013; Sarro *et al.*, 2016; see Table 1 for main findings).

A voxel-based morphometry (VBM) analysis reported a stereotypical AD pattern of parahippocampal atrophy in a small sample of antecedent Aβ-positive patients with Lewy body dementia (Shimada et al., 2013). This observation is broadly consistent with another longitudinal study, where higher baseline levels of global [^{11}C]-PiB binding were associated with higher rates of atrophy in the medial temporal lobe and other cortical regions in DLB over 2 years (Sarro et al., 2016). In both studies, the authors interpreted their findings to suggest that people with DLB may stand to benefit from anti-amyloid therapies should such treatments be available and safe. However, the sample size was rather small in both studies and no controls were recruited (Sarro et al., 2016) Finally, no study has evaluated the relationships of Aβ burden with hippocampal subfields. Post-mortem investigations have demonstrated that hippocampal atrophy in AD is non-uniform, with preferential vulnerability of the cornu ammonis 1 (CA1) and subiculum atrophy in early AD (Braak and Braak, 1991; West et al., 1994). Therefore, understanding how Aβ relates to hippocampal subfields may provide novel insights about the pathological underpinnings of early AD-type atrophy in people with DLB. To these ends, automated techniques have been validated to perform segmentation of hippocampal subfields from structural MRI data (Wisse *et al.*, 2014; Iglesias *et al.*, 2015; Yushkevich *al.*, 2015). We and others have previously applied the Freesurfer technique to demonstrate differential hippocampal subfield atrophy in DLB and AD (Chow et al., 2012; Mak et al., 2016), achieving very similar findings compared to our manual tracing work (Firbank et al., 2010).

To extend these promising investigations and clarify the topography of Aβ-associated atrophy patterns in DLB, we performed a PET-CT and structural MRI study with the following key aims: (a) To compare and

contrast the spatial profiles of abnormal Aβ accumulation and cortical thinning in DLB relative to healthy controls; (b) To determine the global overlap between Aβ binding and cortical thinning, and (c) To delineate the associations of a data-driven composite measure of Aβ burden with regional cortical thickness, hippocampal subfield other subcortical structures.

2. METHODS

2.1. Participants

Participants were recruited prospectively between June 2013 and February 2016 from secondary care services in the North of England. Control subjects were recruited through a research case register or were partners of participants. All subjects were ≥ 60 years old. Dementia subjects had a diagnosis of probable DLB confirmed by two clinicians based on current diagnostic criteria with an MMSE ≥ 12. Results of amyloid imaging were not known to the clinicians when making the diagnosis. Control subjects had an MMSE ≥ 26 and no signs of dementia. DLB subjects were recruited prior to the publication of the 2017 diagnostic criteria for DLB, however, they would satisfy the updated criteria for probable DLB (McKeith et al., 2017). Subjects were excluded if they had a major concurrent psychiatric illness; severe physical illness; contraindications to PET-CT imaging; a history of other significant neurological illness including stroke; previous experimental treatment with an amyloid-targeting agent or current treatment with any other investigational agent. Subjects with capacity gave their written informed consent to take part in the study. For those with dementia who lacked capacity, their participation in the study was discussed with a consultee in accordance with the Mental Capacity Act. The study received ethical approval from the National Research Ethics Service Committee North East - Newcastle & North Tyneside 2 (Research Ethics Committee Identification Number 13/NE/0064).

2.2. Baseline cognitive and clinical assessment

The DLB sample underwent clinical and cognitive assessments, including the Addenbrooke's Cognitive Examination-Revised (ACE-R) and the Revised Unified Parkinson's disease Rating Scale Motor Sub-scale (UPDRS).

2.3. Structural MRI

Scans were acquired on a 3T whole body MR scanner (Achieva scanner; Philips Medical Systems), with body coil transmission and eight channel head coil receiver. Images acquired included a 3D sagittal magnetisation-prepared rapid gradient echo (MPRAGE) sequence (repetition time 8.3ms, echo time 4.6ms, flip angle 8^{o}, inversion delay 1250 ms, imaging time 4.5mins). The sagittal acquisition matrix was 216x240, giving a voxel size of 1x1x1mm. The T1-MPRAGE data were processed using Freesurfer version 6 to obtain cortical thickness measurements in 34 ROIs per hemisphere, based on the Desikan-Killiany parcellation scheme (Desikan et al., 2006). The technical details for the quantification of cortical thickness have been extensively described (Fischl and Dale, 2000). Briefly, for each T1-MPRAGE data, the pial and white matter surfaces were generated and the cortical thickness was measured as the distance between the boundaries of pial and white matter surfaces. Visual inspection was carried by two operators (EM and EMc) while blinded to group diagnostic information, and corrections were performed to ensure accurate skull-stripping, placement of control points and reconstruction of white matter and pial surfaces. Five DLB subjects were excluded in the process. The cortical thickness maps were smoothed using a Gaussian kernel across the surface with a full width at half maximum (FWHM) of 15mm. In addition, the volumetric pipeline of Freesurfer was used to estimate the total intracranial volumes (ICV), as well as the subcortical deep grey matter regions: thalamus, nucleus accumbens, amygdala, pallidum, putamen, caudate and the hippocampus. Hippocampal subfield volumes were estimated using Freesurfer. Briefly, this automated technique uses a probabilistic atlas built upon ultra-high resolution *ex* MRI data (Iglesias et al., 2015). Compared to its previous version (Van Leemput et al., 2009), the ultra-high resolution of the *ex vivo* MRI training data provided a better contrast between the

subfield boundaries, thus improving the reliability of the subfield annotations. As a result, the subfield volumes estimated from this technique yielded better agreement with those from histological studies (Iglesias et al., 2015). To facilitate the integration of PET and MRI data, we used the PetSurfer tool to segment additional regions from the T1 MRI data, such as the cerebral CSF, pons, skull and air cavities. These additional segmentations were merged with the default Freesurfer segmentations to provide anatomical information for partial-volume correction (PVC) described below (Greve et al., 2014).

2.4. PET imaging

PET-CT imaging was performed using a Siemens Biograph-40 PET-CT scanner. Subjects had a 15-minute scan 30-50 minutes after a 370MBq intravenous injection of [^{18}F]-Florbetapir (Amyvid). PET images were reconstructed using iterative reconstruction (4 iterations, 16 subsets), with a 168 x 168 matrix size, 2.04 x 2.04 mm pixel size, 3 mm slice thickness, and 3 mm post-reconstruction Gaussian filter. Attenuation correction was performed utilising CT scan data obtained immediately before the PET images, and reconstructed with 3 mm slice thickness to match the PET images. To perform PVC, each frame of the [^{18}F]-Florbetapir data was realigned with statistical parametric mapping (SPM) and averaged. The resultant mean images were coregistered to their native T1 MRI data and the accuracy of the PET-MRI registration was inspected for each subject. Consistent with previous studies (Greve et al., 2016; LaPoint et al., 2017), the Symmetric Geometric Transfer Matrix (SGTM) technique was implemented to derive PVC-ROIs after the Freesurfer segmentations were transformed back into the PET native space. Subsequently, the standardised uptake ratios (SUVRs) were obtained for each region by normalisation against the cerebellar cortex. Notably, this approach in Freesurfer has been demonstrated to show an excellent agreement of PET regional quantification with manually defined regions (Su et al., 2013). As the SGTM technique is strictly designed for PVC of ROI data, we used the Muller-Gartner technique to perform PVC on vertex-wise [^{18}F]-Florbetapir data (Greve et al., 2014). The corrected vertex-wise PET data were then sampled onto the cortical surface and smoothed using a FWHM of 4 mm. By restricting the smoothing along the cortical ribbon, we further account for the contamination of [^{18}F]-

Florbetapir signal due to contributions from the white matter, CSF or adjacent grey matter regions that are highly proximal in Euclidean space. Compared to volumetric methods, the surface-based PET framework is increasingly advocated for parametric comparisons as it has been associated with reductions of inter-subject variance, and higher reliability across different tracers and PET systems (Greve et al., 2014; Matheson et al., 2017).

2.5. Statistical analyses

Statistical analyses were performed in *MATLAB 2017A* and the *R* statistical package. The specific analyses catering to each of our primary objectives are detailed as follows: To characterise the spatial distribution of increased Aβ and cortical thinning in DLB, both vertex-wise [^{18}F]-Florbetapir PET and cortical thickness data were compared between the DLB and healthy controls using the general linear model in Freesurfer, and were adjusted for age and corrected for multiple comparisons using the cluster-wise method. The vertex-wise threshold, otherwise referred to as the cluster-forming threshold was set at 0.001, while significance for clusters were set $p < 0.05$). Next, using a ROI-based approach, we explored the inter-regional correlation between [^{18}F]-Florbetapir SUVR and cortical thickness (i.e. 68 ROIs per modality) with linear mixed effect models using the *lme4* package in *R* (Bates et al., 2015). Specifically, cortical thickness was assigned as the dependent variable, with [^{18}F]-Florbetapir SUVR ROIs as fixed factors, allowing for random intercepts across subjects and cortical lobes (i.e. frontal, occipital, parietal and temporal lobes) so as to account for the inter-dependency resulting from repeated measurements per subject (i.e. 68 ROIs per subject). The statistical significance of the relationships was assessed using the likelihood ratio test by comparing the fit between the full linear mixed effect model and a reduced model (i.e. without the fixed effect of ^{18}F]-Florbetapir SUVR ROIs (Bates et al., 2015). The [^{18}F]-Florbetapir SUVR dataset across the DLB subjects was first subjected to a principal component analyses (PCA) in order to identify the composite factors that represent the dominant topography of [^{18}F]-Florbetapir SUVR in the DLB sample (i.e. the weighted combination of Aβ binding in brain regions that account for the most variance across the DLB subjects). The resulting score for each DLB

subject could be interpreted as a data-driven composite measure of [^{18}F]-Florbetapir SUVR (Supplementary Fig. 1). Subsequently, the amyloid PCA was correlated with regional cortical thickness (68 ROIs), total hippocampus, CA1 and subiculum while adjusting for age and total intracranial volumes for subcortical volumes. The *a priori* selected hippocampal ROIs were the total hippocampus, CA1 and the total subiculum. To account for multiple correlations, the statistical threshold for significance was set at the Benjamini-Hochberg False Discovery Rate adjusted (FDR) level of $p < 0.05$ (i.e. across 68 ROIs for cortical thickness). The statistical significance threshold was set to $p < 0.05$ for all other tests.

3. RESULTS

3.1. Clinical and demographic information

The brief clinical and cognitive characteristics of the included sample are shown in Table 2. Both the DLB and healthy controls were well-matched in terms of age and gender. As expected, the DLB group scored significantly poorer on the ACER and worse on the UPDRS ($p < 0.001$). To determine whether the exclusion of 5 DLB subjects had a significant impact on the demographics and cognitive characteristics in the study sample, we also compared these variables in the full dataset and found similar results: Both the DLB and healthy control groups were still comparable in terms of age and gender, while MMSE and UPDRS remained significantly poorer in the DLB group ($p < 0.001$) (Supplementary Table 1).

3.2. Vertex-wise comparisons

Compared to the total sample of healthy controls (n = 20), the DLB group demonstrated significantly increased Aβ in widespread regions encompassing the frontal and temporo-parietal cortices (adjusted for age and Monte-Carlo cluster-wise correction: $p_{\text{vertex-wise}} < 0.001$, $p_{\text{cluster-wise}} < 0.05$). Next, we compared cortical thickness in DLB relative to amyloid-negative healthy controls (n = 16). The DLB group showed significant cortical thinning predominantly in the temporal cortex (adjusted for age and Monte-Carlo cluster-wise

correction: $p_{vertex\text{-}wise} < 0.001$, $p_{cluster\text{-}wise} < 0.05$). Both the uncorrected and corrected vertex-wise contrast maps are shown in Figure 1.

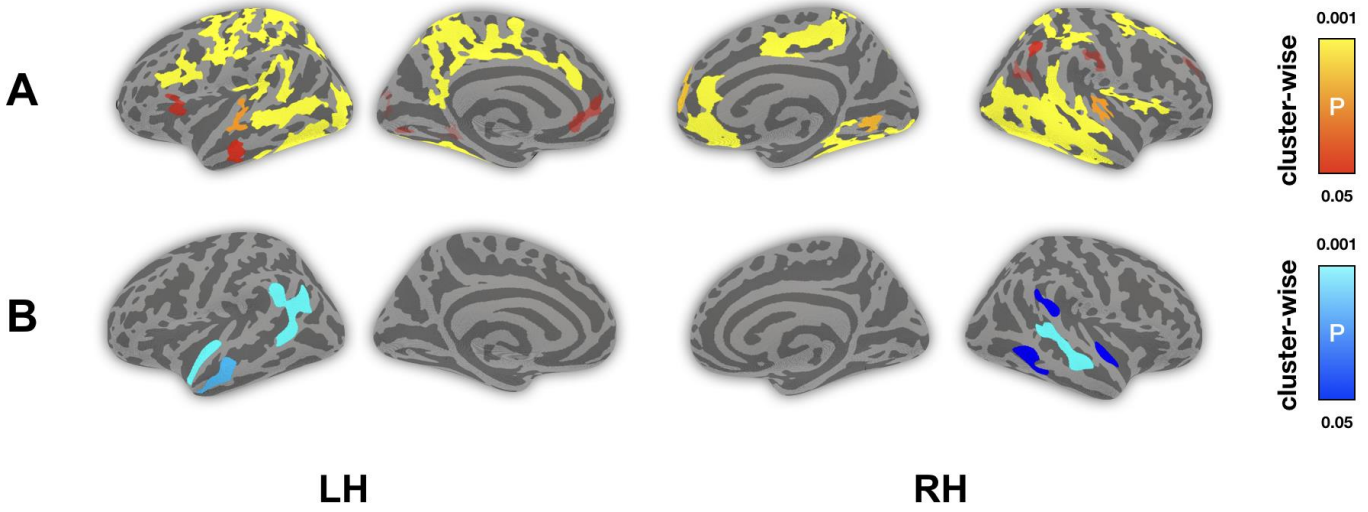

Fig 1. Vertex-wise comparison of [^{18}F]-Florbetapir SUVR and cortical thickness in DLB against healthy controls. A: Compared to controls, DLB showed significantly increased accumulation of Aβ in multiple cortices spanning the frontal and temporo-parietal regions. **B:** Compared to healthy controls, cortical thinning in DLB was restricted to the temporal regions.

3.3. Comparison of total hippocampus and hippocampal subregions

After accounting for age and intracranial volumes, the DLB group showed significantly smaller volumes relative to the amyloid-negative healthy controls in the hippocampus ($p<0.01$) and CA1 ($p=0.02$) and while subiculum differences approached trend ($p = 0.06$) (Fig. 2).

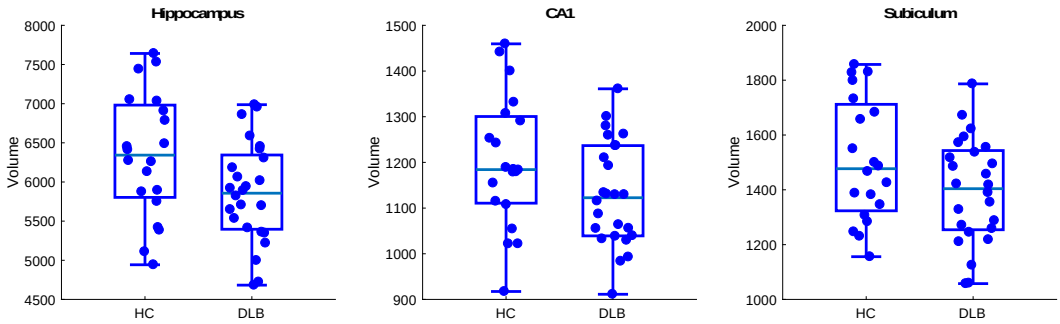

Fig. 2. Boxplot of total volumes in the hippocampus, CA1 and subiculum in DLB and healthy controls. Abbreviations: HC = healthy controls, DLB = dementia with Lewy bodies; CA1 = cornu ammonis 1.

3.4. Global relationship between Aβ and cortical thinning

Mixed effect models showed a weak but significant relationship between [^{18}F]-Florbetapir SUVR and cortical thinning across the cortex in the DLB sample [β = -0.1, SE = 0.02, T = -5.3] (Fig. 3). The statistical significance of this global relationship was inferred from a chi-square comparison of the log-likelihood values against the reduced null model ($p < 0.001$).

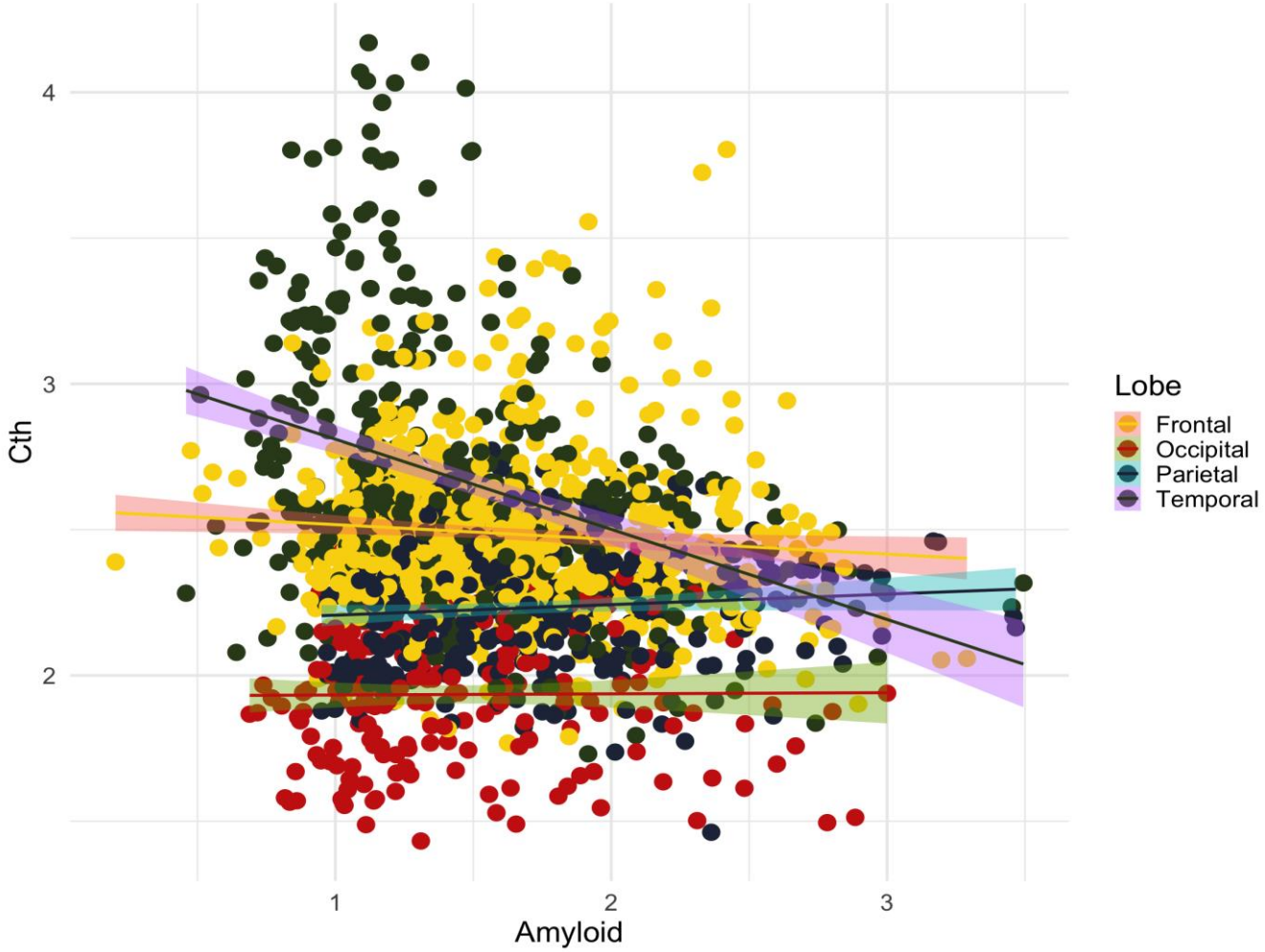

Fig. 3. Global relationship between amyloid and cortical thinning across the cortex. Each data point represents a subject-specific region-of-interest (ROI) from the Desikan-Killiany template (25 DLB subjects * 68 ROIs for amyloid and cortical thickness across the whole brain) and coloured according to the cortical lobes. Mixed effect models revealed a modest but significant relationship between increased [^{18}F]-Florbetapir SUVR and cortical thinning.

3.5. Principal component analysis of [^{18}F]-Florbetapir in DLB and its association with grey matter atrophy

Across the [^{18}F]-Florbetapir SUVRs in the brain regions, PCA was first applied to reduce the dimensionalities of the [^{18}F]-Florbetapir data into component topographies, effectively accounting for the high collinearity of the [^{18}F]-Florbetapir data across ROIs. The PCA revealed a principal Aβ component that was characterised by positive regional loadings in the bilateral precuneus and frontal cortices (79% explained variance) (Fig. 4). We did not find any association of the Aβ principal component with regional cortical thickness after FDR correction. However, it was significantly associated with more severe hippocampal ($r = -0.5$, $p^{FDR} = 0.03$) and subiculum atrophy ($r = -0.6$, $p^{FDR} = 0.01$) after controlling for ICV and age (Fig. 5). To ensure that findings were robust across different techniques, we repeated the analyses using the MGX technique for partial volume correction and obtained consistent results (Supplementary Fig. 3).

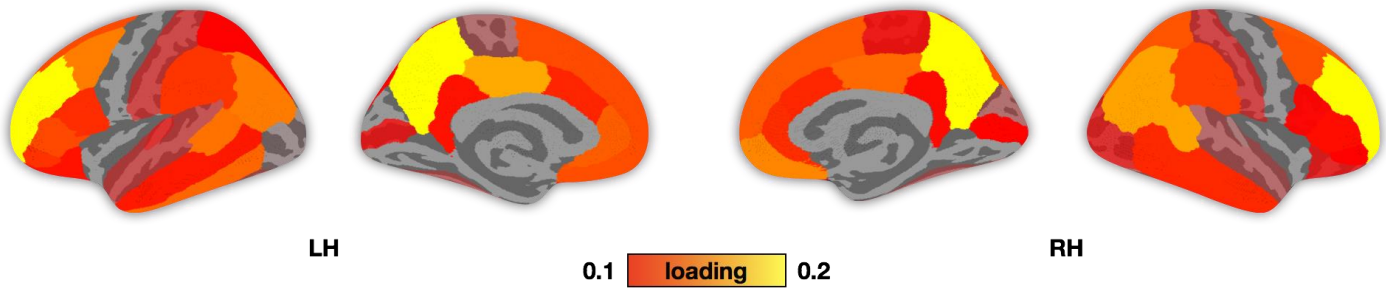

Fig. 4. Multivariate principal component analysis of [^{18}F]-Florbetapir SUVR in DLB. The first identified component of Aβ in DLB explained 79% of the variance. It is characterised by prominent loadings within the bilateral precuneus and frontal cortices, mirroring the characteristic topography of Aβ observed in sporadic AD.

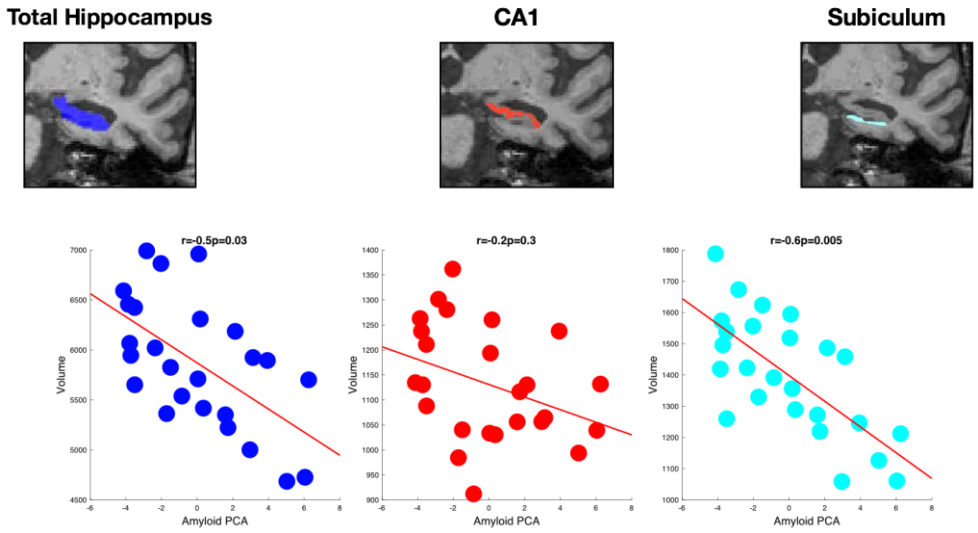

Fig 5. Correlation between Aβ principal component and volume of hippocampal subfields. Across the DLB subjects, greater representation of the Aβ principal component was significantly correlated with smaller hippocampus and subiculum. No signification correlations were found with other subcortical structures.

4. *DISCUSSION*

Clarifying the *in vivo* relationships between Aβ and brain atrophy in DLB will help stratify at-risk persons, and identify vulnerable patients who would stand to benefit from future anti-amyloid therapies should they prove to be effective. To this end, we performed a thorough mapping of Aβ on grey matter atrophy in the largest sample of DLB patients to undergo amyloid PET imaging and structural MRI to date. Overall, our main findings demonstrated that **(a)** the spatial extent of abnormal Aβ accumulation is much wider than the spatial extent of cortical thinning, congruent with conceptual biomarker models that confer primacy of Aβ deposition with respect to brain atrophy; **(b)** the global topography of Aβ showed a modest overlap with cortical thinning across the brain; **(c)** at the regional level, however, Aβ is preferentially associated with hippocampal and subiculum atrophy – both of which are markers of early vulnerability in AD. These findings, along with others (Sarro et al., 2016), appear to support the therapeutic potential of emerging anti-Aβ treatments in DLB.

In our study, the integration of PET and structural MRI data afforded the opportunity to jointly compare the intensity and spatial profiles of abnormal Aβ and cortical thinning within the same DLB subjects against a group of healthy controls who were comparable in terms of age and gender. Our observations of increased Aβ aggregation spanning the inferior temporal, posterior parietal cortices and the medial frontal regions are in accordance with previous studies using the [^{11}C]-PiB tracer (Gomperts et al., 2012, 2008), and together confirm that cortical Aβ is a common feature of DLB that can be detected *in vivo*. In contrast, the pattern of cortical thinning was constrained to the temporal cortex in our sample of DLB. Indeed, the stark disparity between the spatial extent of Aβ accumulation and cortical thinning is in keeping with the biomarker model in AD (Jack et al., 2013).

Set against the putative model of disease progression in AD, we aimed to determine the global overlap between Aβ burden and cortical thinning by using mixed effect models. Interestingly, our whole-brain, inter-regional analyses showed that elevated Aβ binding was associated with cortical thinning particularly in the temporal lobe (Fig. 3), where a focal cluster of significant atrophy was found in DLB compared to healthy controls (Fig. 1). Bearing in mind the absence of a longitudinal design in the present study, it is conceivable that the cortical distribution of antecedent Aβ may shape downstream patterns of cortical thinning in DLB, with the temporal lobe being the most susceptible to the neurotoxicity induced by early Aβ. Nevertheless, the weak effect size of the mixed effect model hints that other pathological factors – such as tau and Lewy bodies – may still influence atrophy to a larger degree than Aβ deposits.

After establishing the topological overlap between increased Aβ binding and cortical thinning, we aimed to determine the extent to which the overall intensity of Aβ is correlated with regional cortical thickness in DLB. Multivariate PCA was first used to identify the most dominant pattern of Aβ in our DLB sample. Unbiased against anatomical definitions, multivariate techniques such as PCA evaluate the covariance structure of the PET data across brain regions rather than proceeding on a region-by-region basis (i.e. conventional univariate

analyses). The principal Aβ component was characterised by higher loadings within the bilateral precuneus and frontal cortices, remarkably mirroring the stereotypical distribution of Aβ in sporadic AD (Brier et al., 2016). This suggests a similar cortical pattern of Aβ binding in DLB and AD, even though absolute levels of Aβ are typically less severe in DLB relative to AD (Donaghy et al., 2015). Consistent with a previous study (Shimada et al., 2016), we did not observe any robust correlations between Aβ and regional cortical thinning. However, the Aβ component was inversely associated with hippocampal and subiculum atrophy – both of which are widely recognised as early structural biomarkers of AD (de Flores *et al.*, 2015; Mak *et al.*, 2017a). This subiculum finding is especially noteworthy considering the growing research interest in hippocampal subfields, which may provide unique disease-related insights beyond the total hippocampus (Firbank *et al.*, 2010; de Flores *et al.*, 2015; Mak *et al.*, 2017b). Indeed, the subicular complex was previously reported as the earliest marker of AD (Carlesimo et al., 2015). Taken together with our findings, DLB patients with greater manifestation of the principal Aβ component are more likely to exhibit atrophy patterns associated with early AD. These findings also confirmed previous reports where higher cortical Aβ was associated with greater temporal lobe atrophy (Sarro et al., 2016; Shimada et al., 2016). Furthermore, the absence of correlations between the Aβ component and other subcortical structures guard against the possibility that our correlational findings are merely reflecting a generalised pattern of Aβ-associated atrophy.

Nevertheless, these cross-sectional correlations should not be taken as evidence for a sole contribution of Aβ to drive atrophy in DLB. Indeed, several lines of research indicate that such conclusions may be oversimplified: **(a)** previous autoradiographic analysis in AD has reported intense tau inclusions ([^{11}C]-PBB3 ligand) in the subiculum *without* noticeable binding of [^{11}C]-PiB (Maruyama et al., 2013); **(b)** we have previously reported that NFTs predicted medial temporal lobe atrophy independent of Aβ plaques in DLB cases (Burton et al., 2009); **(c)** *in vivo* studies in preclinical AD have reported that CSF tau modulates the relationship between Aβ and brain atrophy (Fortea et al., 2014). Furthermore, given the limited spatial resolution of PET, we could not determine whether hippocampal and subiculum atrophy are associated with

focal [^{18}F]-Florbetapir binding within the same regions. Therefore, considering the growing body of evidence implicating early hippocampal and subiculum atrophy in AD (see de Flores *et al.*, 2015 for a systematic review), the present findings may reflect an early process of AD-like atrophy emerging from the synergistic interactions of Aβ and NFTs. Ultimately, longitudinal designs with serial PET imaging of Aβ and NFTs will be necessary to validate this hypothesis.

5. CONCLUSION

Understanding the role of Aβ in people with DLB during life has implications for patient stratification, as well as the optimal design of clinical trials assessing anti-amyloid therapies. In the first report of its kind in DLB, our study demonstrated an association of Aβ with hippocampal and subiculum atrophy in DLB. We propose that Aβ maps onto atrophy in susceptible regions that are amongst the first to undergo neurodegeneration in AD, and concur with previous recommendations for investigating the efficacy of anti-Aβ therapeutics in people with DLB (Gomperts, 2014; Sarro et al., 2016; Shimada et al., 2013). Despite the high-profile failures of anti-Aβ treatments in people with AD, there are several reasons as to why DLB patients may stand to benefit from such treatments. First, it is well-established that macroscopic neurodegeneration is relatively milder in DLB compared to AD (Mak et al., 2015a; Nedelska et al., 2015). To the extent that the effectiveness of disease-modification depends on the preservation of brain structure, it is conceivable that treatments may work better in DLB than in AD, where irreversible and extensive brain atrophy may pose insurmountable challenges for any drug to induce meaningful cognitive benefits. Taking a long-term perspective, future progress in disease-modification trials for AD may also be generalizable for people with DLB, since there is emerging evidence – such as those provided in this study and others – arguing that co-existent Aβ is not a benign process in DLB, but one that may be associated with an AD-type of brain atrophy. Thirdly, clinical trials are warranted to establish whether anti-Aβ treatments could be recommended as an additional intervention as a part of a multi-combinatorial treatment strategy targeting various aspects of DLB. Moving forward, future studies

incorporating multi-PET imaging for tau and alpha-synuclein would be critical to disentangle the respective contributions of different pathologies to the multifaceted clinical picture of DLB.

6. ACKNOWLEDGEMENTS

The authors would like to thank the staff of the NIHR Clinical Research Network North East and Cumbria for their invaluable support with participant recruitment for this study.

7. FUNDING

We thank Avid, a wholly owned subsidiary of Eli Lilly and Company, for supply of Florbetapir and for financial support for the study. This research study was supported by the NIHR Newcastle Biomedical Research Centre.

8. REFERENCES

Bates, D., Mächler, M., Bolker, B., Walker, S., 2015. Fitting Linear Mixed-Effects Models Using lme4. J. Stat. Softw. 67, 1–48. doi:10.18637/jss.v067.i01

Braak, H., Braak, E., 1991. Neuropathological stageing of Alzheimer-related changes. Acta Neuropathol. 82, 239–59.

Brier, M.R., Gordon, B., Friedrichsen, K., McCarthy, J., Stern, A., Christensen, J., Owen, C., Aldea, P., Su, Y., Hassenstab, J., Cairns, N.J., Holtzman, D.M., Fagan, A.M., Morris, J.C., Benzinger, T.L., Ances, B.M., 2016. Tau and A-beta imaging, CSF measures, and cognition in Alzheimer's disease. Sci. Transl. Med. 8, 1–10. doi:10.1126/scitranslmed.aaf2362

Burton, E.J., Barber, R., Mukaetova-Ladinska, E.B., Robson, J., Perry, R.H., Jaros, E., Kalaria, R.N., O'Brien, J.T., 2009. Medial temporal lobe atrophy on MRI differentiates Alzheimer's disease from dementia with Lewy bodies and vascular cognitive impairment: a prospective study with pathological verification of diagnosis. Brain 132, 195–203. doi:10.1093/brain/awn298

Carlesimo, G.A., Piras, F., Orfei, M.D., Iorio, M., Caltagirone, C., Spalletta, G., 2015. Atrophy of presubiculum and subiculum is the earliest hippocampal anatomical marker of Alzheimer's disease. Alzheimer's Dement. (Amsterdam, Netherlands) 1, 24–32. doi:10.1016/j.dadm.2014.12.001

Cash, D.M., Frost, C., Iheme, L.O., ??nay, D., Kandemir, M., Fripp, J., Salvado, O., Bourgeat, P., Reuter, M., Fischl, B., Lorenzi, M., Frisoni, G.B., Pennec, X., Pierson, R.K., Gunter, J.L., Senjem, M.L., Jack, C.R., Guizard, N., Fonov, V.S., Collins, D.L., Modat, M., Cardoso, M.J., Leung, K.K., Wang, H., Das, S.R., Yushkevich, P.A., Malone, I.B., Fox, N.C., Schott, J.M., Ourselin, S., 2015. Assessing atrophy measurement techniques in dementia: Results from the MIRIAD atrophy challenge. Neuroimage 123, 149–164. doi:10.1016/j.neuroimage.2015.07.087

Chetelat, G., La Joie, R., Villain, N., Perrotin, A., De La Sayette, V., Eustache, F., Vandenberghe, R., 2013. Amyloid imaging in cognitively normal individuals, at-risk populations and preclinical Alzheimer's disease. NeuroImage Clin. 2, 356–365. doi:10.1016/j.nicl.2013.02.006

Chetelat, G., Villemagne, V.L., Bourgeat, P., Pike, K.E., Jones, G., Ames, D., Ellis, K.A., Szoeke, C., Martins, R.N., O'Keefe, G.J., Salvado, O., Masters, C.L., Rowe, C.C., 2010. Relationship between atrophy and beta-amyloid deposition in Alzheimer disease. Ann. Neurol. 67, 317–324. doi:10.1002/ana.21955

Chow, N., Aarsland, D., Honarpisheh, H., Beyer, M.K., Somme, J.H., Elashoff, D., Rongve, A., Tysnes, O.B., Thompson, P.M., Apostolova, L.G., 2012. Comparing hippocampal atrophy in Alzheimer's dementia and dementia with lewy bodies. Dement. Geriatr. Cogn. Disord. 34, 44–50. doi:10.1159/000339727

Colom-Cadena, M., Gelpi, E., Charif, S., Belbin, O., Blesa, R., Marti, M.J., Clarimon, J., Lleo, A., 2013. Confluence of alpha-synuclein, tau, and beta-amyloid pathologies in dementia with Lewy bodies. J. Neuropathol. Exp. Neurol. 72, 1203–1212. doi:10.1097/NEN.0000000000000018

de Flores, R., La Joie, R., Landeau, B., Perrotin, A., Mézenge, F., de La Sayette, V., Eustache, F., Desgranges, B., Chételat, G., 2015. Effects of age and Alzheimer's disease on hippocampal subfields.

Hum. Brain Mapp. 36, 463–474. doi:10.1002/hbm.22640

Desikan, R.S., Ségonne, F., Fischl, B., Quinn, B.T., Dickerson, B.C., Blacker, D., Buckner, R.L., Dale, A.M., Maguire, R.P., Hyman, B.T., Albert, M.S., Killiany, R.J., 2006. An automated labeling system for subdividing the human cerebral cortex on MRI scans into gyral based regions of interest. Neuroimage 31, 968–980. doi:10.1016/j.neuroimage.2006.01.021

Donaghy, P., Thomas, A.J., O'Brien, J.T., 2015. Amyloid PET Imaging in Lewy Body Disorders. Am. J. Geriatr. Psychiatry 23, 23–37. doi:10.1016/j.jagp.2013.03.001

Firbank, M.J., Blamire, A.M., Teodorczuk, A., Teper, E., Burton, E.J., Mitra, D., O'Brien, J.T., 2010. High resolution imaging of the medial temporal lobe in Alzheimer's disease and dementia with Lewy bodies. J. Alzheimers. Dis. 21, 1129–40. doi:10.3233/JAD-2010-100138

Fischl, B., Dale, A.M., 2000. Measuring the thickness of the human cerebral cortex from magnetic resonance images. Proc. Natl. Acad. Sci. U. S. A. 97, 11050–5. doi:10.1073/pnas.200033797

Fortea, J., Vilaplana, E., Alcolea, D., Carmona-Iragui, M., Sánchez-Saudinos, M.B., Sala, I., Antón-Aguirre, S., González, S., Medrano, S., Pegueroles, J., Morenas, E., Clarimón, J., Blesa, R., Lleó, A., 2014. Cerebrospinal fluid β-amyloid and phospho-tau biomarker interactions affecting brain structure in preclinical Alzheimer disease. Ann. Neurol. 76, 223–230. doi:10.1002/ana.24186

Gomperts, S.N., 2014. Imaging the role of amyloid in PD dementia and dementia with Lewy bodies. Curr. Neurol. Neurosci. Rep. 14. doi:10.1007/s11910-014-0472-6

Gomperts, S.N., Locascio, J.J., Marquie, M., Santarlasci, A.L., Rentz, D.M., Maye, J., Johnson, K.A., Growdon, J.H., 2012. Brain amyloid and cognition in Lewy body diseases. Mov. Disord. 27, 965–973. doi:10.1002/mds.25048

Gomperts, S.N., Rentz, D.M., Moran, E., Becker, J.A., Locascio, J.J., Klunk, W.E., Mathis, C.A., Elmaleh, D.R., Shoup, T., Fischman, A.J., Hyman, B.T., Growdon, J.H., Johnson, K.A., 2008. Imaging amyloid deposition in Lewy body diseases. Neurology 71, 903–10. doi:10.1212/01.wnl.0000326146.60732.d6

Greve, D.N., Salat, D.H., Bowen, S.L., Izquierdo-Garcia, D., Schultz, A.P., Catana, C., Becker, J.A., Svarer,

C., Knudsen, G.M., Sperling, R.A., Johnson, K.A., 2016. Different partial volume correction methods lead to different conclusions: An 18F-FDG-PET study of aging. Neuroimage 132, 334–343. doi:10.1016/j.neuroimage.2016.02.042

Greve, D.N., Svarer, C., Fisher, P.M., Feng, L., Hansen, A.E., Baare, W., Rosen, B., Fischl, B., Knudsen, G.M., 2014. Cortical surface-based analysis reduces bias and variance in kinetic modeling of brain PET data. Neuroimage 92, 225–236. doi:10.1016/j.neuroimage.2013.12.021

Habib, M., Mak, E., Gabel, S., Su, L., Williams, G., Waldman, A., Wells, K., Ritchie, K., Ritchie, C., O'Brien, J.T., 2017. Functional neuroimaging findings in healthy middle-aged adults at risk of alzheimer's disease. Ageing Res. Rev. doi:10.1016/j.arr.2017.03.004

Hardy, J., 2002. The Amyloid Hypothesis of Alzheimer's Disease: Progress and Problems on the Road to Therapeutics. Science (80-.). 297, 353–356. doi:10.1126/science.1072994

Iglesias, J.E., Augustinack, J.C., Nguyen, K., Player, C.M., Player, A., Wright, M., Roy, N., Frosch, M.P., McKee, A.C., Wald, L.L., Fischl, B., Van Leemput, K., 2015. A computational atlas of the hippocampal formation using ex vivo, ultra-high resolution MRI: Application to adaptive segmentation of in vivo MRI. Neuroimage 115, 117–137. doi:10.1016/j.neuroimage.2015.04.042

Jack, C.R., Knopman, D.S., Jagust, W.J., Petersen, R.C., Weiner, M.W., Aisen, P.S., Shaw, L.M., Vemuri, P., Wiste, H.J., Weigand, S.D., Lesnick, T.G., Pankratz, V.S., Donohue, M.C., Trojanowski, J.Q., 2013. Tracking pathophysiological processes in Alzheimer's disease: an updated hypothetical model of dynamic biomarkers. Lancet Neurol. 12, 207–216. doi:10.1016/S1474-4422(12)70291-0

Josephs, K. a., Whitwell, J.L., Ahmed, Z., Shiung, M.M., Weigand, S.D., Knopman, D.S., Boeve, B.F., Parisi, J.E., Petersen, R.C., Dickson, D.W., Jack, C.R., 2008. Beta-Amyloid Burden Is Not Associated With Rates of Brain Atrophy. Ann. Neurol. 63, 204–212. doi:10.1002/ana.21223

LaPoint, M.R., Chhatwal, J.P., Sepulcre, J., Johnson, K.A., Sperling, R.A., Schultz, A.P., 2017. The association between tau PET and retrospective cortical thinning in clinically normal elderly. Neuroimage. doi:10.1016/j.neuroimage.2017.05.049

Mak, E., Gabel, S., Mirette, H., Su, L., Williams, G.B., Waldman, A., Wells, K., Ritchie, K., Ritchie, C., O'Brien, J., 2017a. Structural neuroimaging in preclinical dementia: From microstructural deficits and grey matter atrophy to macroscale connectomic changes. Ageing Res. Rev. 35, 250–264. doi:10.1016/j.arr.2016.10.001

Mak, E., Gabel, S., Su, L., Williams, G.B., Arnold, R., Passamonti, L., Rodríguez, P.V., Surendranathan, A., Bevan-jones, W.R., Rowe, J.B., O'Brien, J.T., 2017b. Multi-modal MRI investigation of volumetric and microstructural changes in the hippocampus and its subfields in mild cognitive impairment , Alzheimer ' s disease , and dementia with Lewy bodies. Int. Psychogeriatrics 29, 545–555. doi:10.1017/S1041610216002143

Mak, E., Su, L., Williams, G.B., Watson, R., Firbank, M., Blamire, A., O'Brien, J., 2016. Differential Atrophy of Hippocampal Subfields: A Comparative Study of Dementia with Lewy Bodies and Alzheimer Disease. Am. J. Geriatr. Psychiatry 24, 136–143. doi:10.1016/j.jagp.2015.06.006

Mak, E., Su, L., Williams, G.B., Watson, R., Firbank, M., Blamire, A.M., O'Brien, J.T., 2015. Longitudinal assessment of global and regional atrophy rates in Alzheimer's disease and dementia with Lewy bodies. NeuroImage Clin. 7, 456–462. doi:10.1016/j.nicl.2015.01.017

Maruyama, M., Shimada, H., Suhara, T., Shinotoh, H., Ji, B., Maeda, J., Zhang, M.R., Trojanowski, J., Lee, V.Y., Ono, M., Masamoto, K., Takano, H., Sahara, N., Iwata, N., Okamura, N., Furumoto, S., Kudo, Y., Chang, Q., Saido, T., Takashima, A., Lewis, J., Jang, M.K., Aoki, I., Ito, H., Higuchi, M., 2013. Imaging of tau pathology in a tauopathy mouse model and in alzheimer patients compared to normal controls. Neuron 79, 1094–1108. doi:10.1016/j.neuron.2013.07.037

Matheson, G.J., Stenkrona, P., Cselényi, Z., Plavén-sigray, P., Halldin, C., Farde, L., Cervenka, S., 2017. Reliability of volumetric and surface-based normalisation and smoothing techniques for PET analysis of the cortex: A test-retest analysis using [11C]SCH-23390. Neuroimage 155, 344–353. doi:10.1016/j.neuroimage.2017.04.031

McKeith, I.G., Boeve, B.F., Dickson, D.W., Halliday, G., Aarsland, D., Attems, J., Ballard, C.G., Bayston,

A., Beach, T.G., Chen-plotkin, A., Singleton, A., Taylor, A., 2017. Diagnosis and management of dementia with Lewy bodies: Fourth consensus report of the DLB Consortium. Neurology 89, 1–13.

McKeith, I.G., Dickson, D.W., Lowe, J., Emre, M., O'Brien, J.T., Feldman, H., Cummings, J., Duda, J.E., Lippa, C., Perry, E.K., Aarsland, D., Arai, H., Ballard, C.G., Boeve, B., Burn, D.J., Costa, D., Del Ser, T., Dubois, B., Galasko, D., Gauthier, S., Goetz, C.G., Gomez-Tortosa, E., Halliday, G., Hansen, L.A., Hardy, J., Iwatsubo, T., Kalaria, R.N., Kaufer, D., Kenny, R.A., Korczyn, A., Kosaka, K., Lee, V.M.Y., Lees, A., Litvan, I., Londos, E., Lopez, O.L., Minoshima, S., Mizuno, Y., Molina, J.A., Mukaetova-Ladinska, E.B., Pasquier, F., Perry, R.H., Schulz, J.B., Trojanowski, J.Q., Yamada, M., Consortium on DLB, 2005. Diagnosis and management of dementia with Lewy bodies: Third report of the DLB consortium. Neurology 65, 1863–1872. doi:10.1212/01.wnl.0000187889.17253.b1

Nedelska, Z., Ferman, T.J., Boeve, B.F., Przybelski, S.A., Lesnick, T.G., Murray, M.E., Gunter, J.L., Senjem, M.L., Vemuri, P., Smith, G.E., Geda, Y.E., Graff-Radford, J., Knopman, D.S., Petersen, R.C., Parisi, J.E., Dickson, D.W., Jack, C.R., Kantarci, K., 2015. Pattern of brain atrophy rates in autopsy-confirmed dementia with Lewy bodies. Neurobiol. Aging. doi:10.1016/j.neurobiolaging.2014.07.005

Sarro, L., Senjem, M.L., Lundt, E.S., Przybelski, S.A., Lesnick, T.G., Graff-Radford, J., Boeve, B.F., Lowe, V.J., Ferman, T.J., Knopman, D.S., Comi, G., Filippi, M., Petersen, R.C., Jack, C.R., Kantarci, K., 2016. Amyloid-β deposition and regional grey matter atrophy rates in dementia with Lewy bodies. Brain 139, 2740–2750. doi:10.1093/brain/ww193

Schott, J.M., Bartlett, J.W., Barnes, J., Leung, K.K., Ourselin, S., Fox, N.C., 2010. Reduced sample sizes for atrophy outcomes in Alzheimer's disease trials: Baseline adjustment. Neurobiol. Aging 31, 1452–1462.e2. doi:10.1016/j.neurobiolaging.2010.04.011

Shimada, H., Kitamura, S., Shinotoh, H., Endo, H., Niwa, F., Hirano, S., Kimura, Y., Zhang, M.-R., Kuwabara, S., Suhara, T., Higuchi, M., 2016. Association between Aβ and tau accumulations and their influence on clinical features in aging and Alzheimer disease spectrum brains: A [11C]PBB3-PET study. Alzheimer's Dement. Diagnosis, Assess. Dis. Monit. 6, 11–20. doi:10.1016/j.dadm.2016.12.009

Shimada, H., Shinotoh, H., Hirano, S., Miyoshi, M., Sato, K., Tanaka, N., Ota, T., Fukushi, K., Irie, T., Ito, H., Higuchi, M., Kuwabara, S., Suhara, T., 2013. Beta-amyloid in lewy body disease is related to Alzheimer's disease-like atrophy. Mov. Disord. 28, 169–175. doi:10.1002/mds.25286

Slattery, C.F., Zhang, J., Paterson, R.W., Foulkes, A.J.M., Mancini, L., Thomas, D.L., Modat, M., Toussaint, N., Cash, D.M., Thornton, J.S., Alexander, D.C., Ourselin, S., Fox, N.C., Zhang, H., Schott, J.M., 2015. Neurite orientation dispersion and density imaging (NODDI) in young-onset Alzheimer's disease and its syndromic variants. Alzheimer's Dement. 11, P91. doi:10.1016/j.jalz.2015.06.156

Sluimer, J.D., van der Flier, W.M., Karas, G.B., Fox, N.C., Scheltens, P., Barkhof, F., Vrenken, H., 2008. Whole-brain atrophy rate and cognitive decline: longitudinal MR study of memory clinic patients. Radiology 248, 590–598. doi:10.1148/radiol.2482070938

Sperling, R.A., Rentz, D.M., Johnson, K.A., Karlawish, J., Donohue, M., Salmon, D.P., Aisen, P., 2014. The A4 study: stopping AD before symptoms begin? Sci. Transl. Med. 6, 228fs13. doi:10.1126/scitranslmed.3007941

Su, Y., D'Angelo, G.M., Vlassenko, A.G., Zhou, G., Snyder, A.Z., Marcus, D.S., Blazey, T.M., Christensen, J.J., Vora, S., Morris, J.C., Mintun, M.A., Benzinger, T.L.S., 2013. Quantitative analysis of PiB-PET with FreeSurfer ROIs. PLoS One 8. doi:10.1371/journal.pone.0073377

Van Leemput, K., Bakkour, A., Benner, T., Wiggins, G., Wald, L.L., Augustinack, J., Dickerson, B.C., Golland, P., Fischl, B., 2009. Automated segmentation of hippocampal subfields from ultra-high resolution in vivo MRI. Hippocampus 19, 549–57. doi:10.1002/hipo.20615

West, M.., Coleman, P.., Flood, D.., Troncoso, J.., 1994. Differences in the pattern of hippocampal neuronal loss in normal ageing and Alzheimer's disease. Lancet 344, 769–772. doi:10.1016/S0140-6736(94)92338-8

Wisse, L.E.M., Biessels, G.J., Heringa, S.M., Kuijf, H.J., Koek, D.L., Luijten, P.R., Geerlings, M.I., 2014. Hippocampal subfield volumes at 7T in early Alzheimer's disease and normal aging. Neurobiol. Aging 35, 2039–2045. doi:10.1016/j.neurobiolaging.2014.02.021

Yushkevich, P.A., Pluta, J.B., Wang, H., Xie, L., Ding, S.-L., Gertje, E.C., Mancuso, L., Kliot, D., Das, S.R., Wolk, D.A., 2015. Automated volumetry and regional thickness analysis of hippocampal subfields and medial temporal cortical structures in mild cognitive impairment. Hum. Brain Mapp. 36, 258–287. doi:10.1002/hbm.22627

Authors	**Sample characteristics**	**Study design and imaging analyses**	**Summary of main findings**
Shimada et al., 2013	17 HC Age: 68, MMSE: 28 8 DLB, 7 PDD Age: 73, MMSE: 22 13 AD Age: 76, MMSE: 20	Cross-sectional analysis Voxel-based morphometry Partial volume was not performed on [^{11}C]-PiB data	Aβ+ DLB/PDD subjects showed parahippocampal, lateral temporal and parietal atrophy. Aβ- DLB/PDD did not exhibit significant atrophy. Mean [^{11}C]-PiB SUVR did not correlate with voxel-wise grey matter maps.
Sarro et al., 2016	20 DLB Age: 70, MMSE: 22	Longitudinal within-group design Time between MRI scans: 2.5 years ROI analysis between global [^{11}C]-PiB uptake and rate of atrophy in grey matter ROIs, controlled for age	Higher baseline [^{11}C]-PiB SUVR was associated with accelerated GM atrophy over time in multiple regions, such as the posterior cingulate cortex, medial temporal lobe, occipital lobe, caudate and putamen, and ventricular enlargement

Table 1. Summary of main findings from previous studies investigating the association of [^{11}C]-PiB binding to grey matter atrophy in DLB. Abbreviations: Aβ = beta-amyloid; HC = Healthy controls; DLB = Dementia with Lewy bodies; PDD = Parkinson's disease with dementia; VBM = Voxel-based morphometry; ROI = Region of interest; MMSE = Mini-mental state examination; MRI = Magnetic resonance imaging; PiB = Pittsburgh Compound B.

	Controls (n=20)	**DLB (n=25)**	**P value**
Age	75.9 ± 7.3	75.4 ± 6.8	0.8 †
Gender (male:female)	16:4	21:4	0.7 [c]
ACER	94.8 ± 3.02	65 ± 15.2	< 0.001 [r]
UPDRS	5.6 ± 3.5	41.5 ± 19.0	< 0.001 [r]
Disease duration (months)	n/a	19.4 ± 13.5	
Aβ positivity	4	13	

Table 2. Brief demographics and cognitive characteristic of the study sample. Abbreviations: ACER = Addenbrooke's Cognitive Examination Revised, UPDRS = Revised Unified Parkinson's disease Rating Scale Motor Sub-scale; DLB = Dementia with Lewy bodies; † = Student's T-Test; [C] = Chi-squared test; [R] = Rank-sum test.